Chemistry–A European Journal
Research Article
doi.org/10.1002/chem.202300405
Chemistry Europe
European Chemical Societies Publishing
www.chemeurj.org

Ruthenium Complexes of Polyfluorocarbon Substituted Terpyridine and Mesoionic Carbene Ligands: An Interplay in CO_2 Reduction

Felix Stein[+],[a, b] Maite Nößler[+],[a] Arijit Singha Hazari,*[b] Lisa Böser,[a] Robert Walter,[b] Hang Liu,[c] Elias Klemm,[c] and Biprajit Sarkar*[a, b]

Abstract: In recent years terpyridines (tpy) and mesoionic carbenes (MIC) have been widely used in metal complexes. With the right combination with a metal center, both of these ligands are individually known to generate excellent catalysts for CO_2 reduction. In this study, we combine the potentials of PFC (PFC = polyfluorocarbon) substituted tpy and MIC ligands within the same platform to obtain a new class of complexes, which we investigated with respect to their structural, electrochemical and UV/Vis/NIR spectroelectrochemical properties. We further show that the resulting metal complexes are potent electrocatalysts for CO_2 reduction in which CO is exclusively formed with a faradaic efficiency of 92%. A preliminary mechanistic study, including the isolation and characterization of a key intermediate is also reported.

Introduction

The increasing demand for energy and the threat of climate change show the need to further develop energy sources. One of the current focus is the study of molecular electrocatalysts for downstream reactions to new energy technologies.[1] In this regard, proton or oxygen reduction, water oxidation, or CO_2 reduction are a research focus because they involve the release or storage of energy.[2,3] One of the most important atmospheric gases contributing to the greenhouse effect is CO_2, and because it is the major source of carbon, its electrochemical reduction into fuels has attracted considerable interest.[4]

The selective electrochemical CO_2 reduction is still a subject of research despite extensive investigations in the last decades due to the high overpotential of the cathodic process.[2,5] One of the most prominent approaches to maximizing the catalytic activity of molecular electrocatalysts is to tune the electronic properties of the ligands.[6] For example, placement of a strong electron donating ligand increases the CO_2 activation rate, by making the metal center more nucleophilic.[7] However, this leads to an undesirable increase in the overpotential, since a stronger electron donating ligand typically leads to a more negative reduction potential.[8] The development of a catalyst, in which the kinetics of the chemical steps and the reduction potentials are controlled by two different ligands is one approach to solving this problem.[9] In this context, Miller and co-workers investigated ruthenium(II) complexes bearing a terpyridine and a bidentate pyridyl-NHC ligand, and showed an impact of the *trans* effect on the electrocatalysis.[8,9] More recently, the same group has reported on iron(II) and ruthenium(II) complexes with terpyridine and chelating bi-NHC ligands as electrocatalysts for CO_2 reduction.[10]

One way to control the reduction potential is to introduce highly tunable tridentate N-containing terpyridine (tpy) ligands, which is frequently used in coordination chemistry. Ruthenium(II) complexes of terpyridines have been intensively studied, as they exhibit well-defined electrochemical and photochemical properties and are also used in various catalytic processes[11,12] such as proton and CO_2 reduction,[13] or water oxidation.[14] However, the synthesis of structurally diverse terpyridine ligands, for example, those with electronically different substituents, still remains a challenge.[15]

Currently, mesoionic carbene (MIC) ligands are of great interest in organometallic chemistry, due to their strong donor properties and unusual bonding situation.[16,17] They can be synthesized by the copper(I)-catalyzed azide–alkyne cycloaddition reaction, which is facile and modular.[18] A large number of complexes have already been reported with these ligands, especially with the late transition metals.[19,20,21] For the generation of metal complexes with intriguing electrochemical and photochemical properties, MICs are a preferred class of

[a] F. Stein,[+] M. Nößler,[+] L. Böser, Prof. Dr. B. Sarkar
Institut für Chemie und Biochemie
Anorganische Chemie
Freie Universität Berlin
Fabeckstraße 34–36, 14195, Berlin (Germany)
[b] F. Stein,[+] Dr. A. S. Hazari, R. Walter, Prof. Dr. B. Sarkar
Institut für Anorganische Chemie
Universität Stuttgart
Pfaffenwaldring 55, 70569 Stuttgart (Germany)
E-mail: biprajit.sarkar@iac.uni-stuttgart.de
[c] Dr. H. Liu, Prof. Dr. E. Klemm
Institut für Technische Chemie
Universität Stuttgart
Pfaffenwaldring 55, 70569 Stuttgart (Germany)
[+] These authors contributed equally to this work.

Supporting information for this article is available on the WWW under https://doi.org/10.1002/chem.202300405

ligands.[16,20,21] Moreover, the corresponding metal complexes can be used in homogeneous catalysis.[22] Furthermore, MICs have recently shown great potential as powerful ligands for generating metal complexes for electrocatalysis with relevance to energy related research.[23]

In this work, we present different ruthenium(II) complexes bearing a MIC ligand and tpy ligands with an incorporated perfluorocarbon chain (PFC) at the tail (Figure 1). The MIC ligands which are more strongly donating than the NHCs are used for controlling kinetics of electrocatalytic CO_2 reduction,[16,17,19–21,24] and the PFC tail in the tpy ligand for controlling the overpotential. The influence of the PFC tail on the overpotential for electrochemical CO_2 reduction is investigated. As the different chain-length of the PFC tail is expected to have an influence on the tpy based reduction process, we were interested in deciphering how these substitution patterns would influence the tuning of the overpotential in electrochemical CO_2 reduction with such complexes. Additionally, the chloride ligand is labile and provides a readily available vacant site for CO_2 binding. These complexes were studied electrochemically by cyclic voltammetry and UV/Vis/NIR-spectroelectrochemistry. In addition, metal complexes of these frameworks are investigated as electrocatalysts for CO_2 reduction together with a first mechanistic study. To the best of our knowledge, this is the first time that a MIC ligand is combined with a tpy ligand bearing a PFC tail.

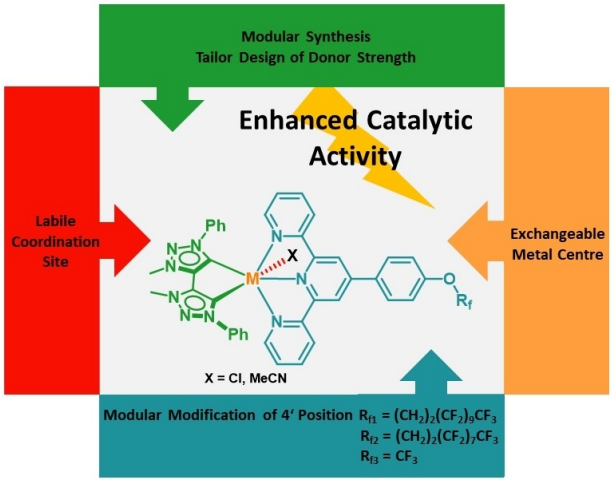

Figure 1. Synthetic access for the development of a molecular catalyst for the electrocatalytic CO_2 reduction.

Results and Discussion

Synthesis and structural characterization

The synthesis of the terpyridine ligands (tpy, **L1**-**L3**) with different per fluorinated alkyl chains as well as the ruthenium complex with cymene (**Ru_1**) and a bis MIC-ligand were recently developed by us.[25] To obtain the mixed ruthenium complexes with substituted terpyridine and MIC ligands (**Ru_2**-**Ru_4**), **Ru_1** was reacted with the respective terpyridines (**L_1**-**L_3**) in DMSO at 120 °C (Scheme 1). After chromatographic work up, we were able to isolate the complexes in moderate to good yields.[26] The corresponding acetonitrile complex **Ru_5** was synthesized by reacting **Ru_4** with $AgPF_6$ in acetonitrile in 95% yield (Scheme 2). The facile synthesis of **Ru_5** under ambient conditions already points to a somewhat labile Ru–Cl bond, as would be expected owing to the strong donor properties of the MIC–C donor that

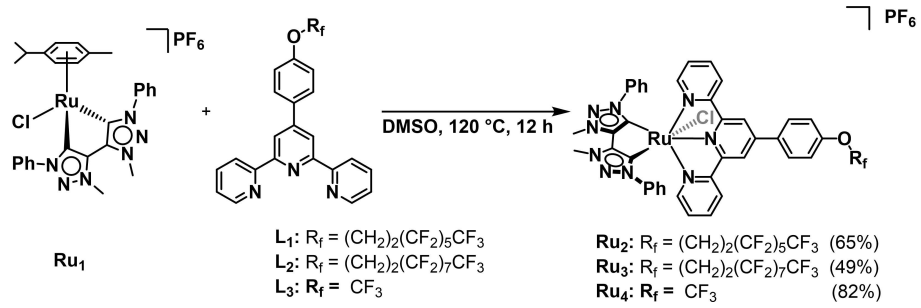

Scheme 1. Synthesis of the ruthenium complexes **Ru_2**-**Ru_4**.

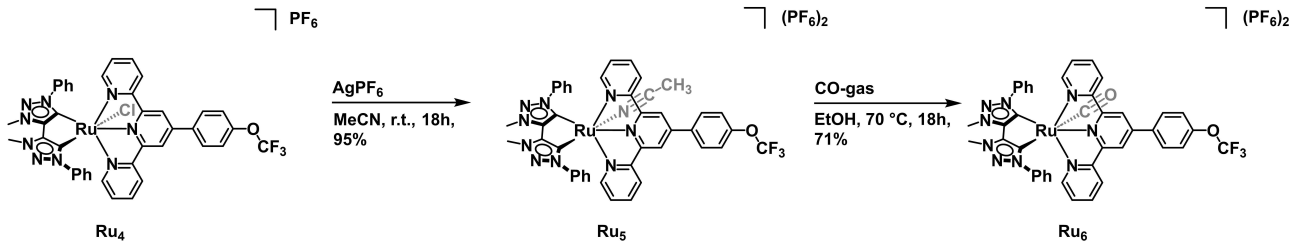

Scheme 2. Synthesis of the ruthenium complexes **Ru_5** and **Ru_6**.

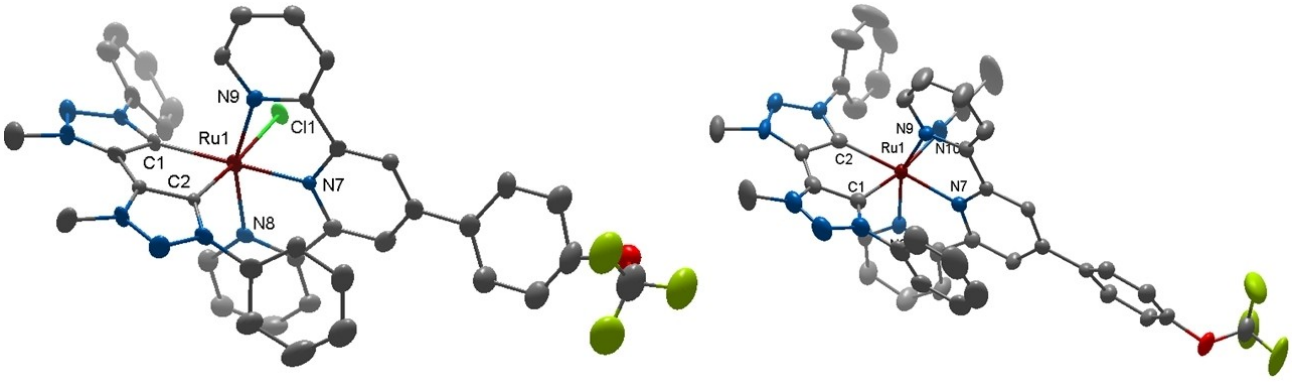

Figure 2. Perspective view of complex Ru_4 and Ru_5. Ellipsoids are at a probability level of 50 %. H atoms, anions and disordered atoms are omitted for clarity.

is trans to the chlorido ligand in complex Ru_4. This fact is expected to be beneficial in the use of Ru_4 as an electrocatalyst (see below). Starting from Ru_5, the exchange of the acetonitrile with an CO was performed in ethanol under an atmosphere of CO gas at 70 °C. The formation of the desired complexes Ru_6 was indicated by a color change from brownish to intense yellow. An intense peak at 1994 cm^{-1} in the IR-spectrum for the Ru-CO stretching frequency and the characteristic peak in the ^{13}C NMR spectrum at 194.8 ppm for the carbon atom of the CO confirms the generation of the desired complex. The aforementioned values fit well with data for related compounds reported in the literature (Figure S14 and S37).[27] All the complexes were characterized by NMR spectroscopy, mass spectrometry and elemental analysis (see Supporting Information).

The ^1H NMR spectra of all complexes show well defined signals in the expected region. The two resonances corresponding to the two methyl groups of the MIC ligands are in the typical range between 4.8 ppm and 4.5 ppm. All the signals in the aromatic region assigned to the tpy are shifted high field, compared to the free ligand, confirming the coordination to the ruthenium center. ^{13}C NMR spectra show typical resonances between 191 ppm and 183 ppm for metal bound carbene carbons. The specific signals for all the complexes in the ^{19}F NMR are a further proof for the formation of the desired complex (Figures S1–S17, see Supporting Information).

The molecular structures of Ru_4 and Ru_5 in the crystal were investigated from single crystal X-ray diffraction studies (XRD). Unfortunately, it was not possible to grow suitable single crystals for the other two complexes with longer chain length, which is probably due to the precipitation problem. This phenomena has already been described previously in the literature.[9]

Complex Ru_4 crystallizes in a triclinic $P\bar{1}$ space group. The ruthenium center is coordinated in a pseudo-octahedral fashion through three nitrogen atoms of the tpy ligand, two carbon atoms of the MIC ligand and the chloride. The Ru–N7 bond lengths to the central ring of the tridentate ligand is shorter than the bond lengths Ru–N8 and Ru–N9 to the terminal rings (Figure 2 and Table 1). This could be due to the rigidity of the ligands that prevent the three donor atoms of the same tpy ligand from approaching the ruthenium center equally closely.[12] The rings of the MIC ligand are slightly out of plane and the two phenyl rings are also rotated out of plane. The connectivity and geometry of the nitrile complex Ru_5 obtained by replacing the chloride with an acetonitrile was further approved with the solid structure. The Ru–C1 bond length is similar with Ru_4. As expected, the Ru–C2 bond length (Figure 2) is elongated by ca. 0.07 Å, due to changing donor ability from chloride to acetonitrile. This trend can also be seen in the elongation of the ruthenium nitrogen bond of the terpyridine.

Table 1. Selected bond lengths in [Å] from measurements at 100 K.

Bond	Ru_4	Ru_5
Ru–N7	1.972(8)	1.995(2)
Ru–N8	2.055(8)	2.073(2)
Ru–N9	2.066(8)	2.084(2)
Ru–C1	2.077(9)	2.069(3)
Ru–C2	2.013(9)	2.084(2)
Ru–Cl1	2.472(2)	-
Ru–N (MeCN)	-	2.088(2)

Electrochemistry

The electrochemical properties of the complexes were evaluated via cyclic voltammetric analysis in acetonitrile solution with 0.1 M tetrabutylammonium hexafluorophosphate (NBu_4PF_6) as the supporting electrolyte, at 100 mV/s scan rate. Table 2 summarizes electrochemical potentials of all the complexes. Investigation of cyclic voltammograms of all the

Table 2. Redox potentials of the complexes referenced against Fc/FcH^+ redox couple measured in acetonitrile at room temperature.[a]

	$E^{Ox2}_{1/2}$ [V]	$E^{Ox1}_{1/2}$ [V]	$E^{Red1}_{1/2}$ [V]	$E^{Red2}_{1/2}$ [V]	$E^{Red3}_{1/2}$ [V]
Ru_2[b]	0.450	0.07	−1.84	−2.00	−2.37
Ru_3	0.453	0.14	−1.85	−2.00	−2.30
Ru_4	0.482	0.06	−1.79	−1.96	−2.29

[a] All measured with a glassy carbon electrode. [b] Irreversible, forward peak potential.

complexes revealed a reversible 1e$^-$ oxidation and reduction (ΔE_p ~71 mV) for **Ru_4**, in contrary to the irreversible redox processes in the case of **Ru_2** containing octyl PFC tail, as illustrated in the Figure 3. Irreversibility of the redox process could be ascribed to the adsorption of the reduced species on the electrode bearing resemblance to the previously reported ruthenium terpyridine and electron donating ligands.[11] Interestingly, **Ru_3**, the higher analogue of **Ru_2** exhibited two and one reversible 1e$^-$ oxidation and reduction processes respectively along with two quasireversible reduction waves (Figure 3). Based on the Mulliken spin population and literature reports on the similary type of complexes, first reduction process can be assigned to terpyridine based, while second and third reduction processes are most likely focused on the MIC and terpyridine center, respectively. On the other hand, greater contribution of the metal center to the overall spin population on oxidation in **Ru_2** and **Ru_3** indicate metal-centered oxidation process Ru^{II}/Ru^{III}).

Comparison of the redox potentials revealed no significant influence of the increasing chain length of the PFC tail at the peripheral position of the terpyridine ring. Scan dependent sweep of the potentials exhibited linear dependence of the peak current on the square root of the scan rate indicating a diffusion-controlled process, as illustrated in Figure 4 for **Ru_4**.

Cyclic voltammograms of the corresponding acetonitrile solvated complex **Ru_5** was also investigated in acetonitrile solution with 0.1 M tetrabutylammonium hexafluorophosphate (NBu_4PF_6) as the supporting electrolyte, at 100 mV/s scan rate (Figure S21). The complex displayed one reversible and multiple quasi-reversible redox processes with an irreversible process near to 0 V. This irreversible wave could be due to the adsorption of the complex at the surface of the working electrode. To address the problem, cyclic voltammetry was measured under an identical experimental condition replacing NBu_4PF_6 with tetrabutylammonium chloride (NBu_4Cl) as the supporting electrolyte to form an equilibrium between the chloride containing complex **Ru_4** and the complex **Ru_5** (Figure S21). The voltammograms displayed multiple redox processes without any irreversible process indicating an equilibrium between chloride and acetonitrile ligand in the presence of higher concentrations of chloride ion, and indicating the presence of a labile coordination site in **Ru_5** as the possible reason for the adsorption peak close of 0 V for **Ru_5**.

UV/Vis/NIR spectroelectrochemistry (UV/Vis-SEC)

The UV/Vis spectra of the complexes were recorded in acetonitrile. For **Ru4**, an immediate color change of the solution from intense purple to brownish/orange was observed. This could be followed from the UV/Vis spectra (Figure 5) by a red shift of the absorption band at 478 nm to 545 nm. If the solvent is removed and the remaining solid is dissolved in DCM or THF, the color of the solution turns intense purple again. The band in the visible region can be assigned to metal to ligand charge transfer (MLCT), which was further confirmed by DFT calculations (Figure S41). The absorption band at 326 nm is due to the MLCT from the ruthenium to the terminal pyridine rings of the tpy. The intense absorption in the UV region at 283 nm is a

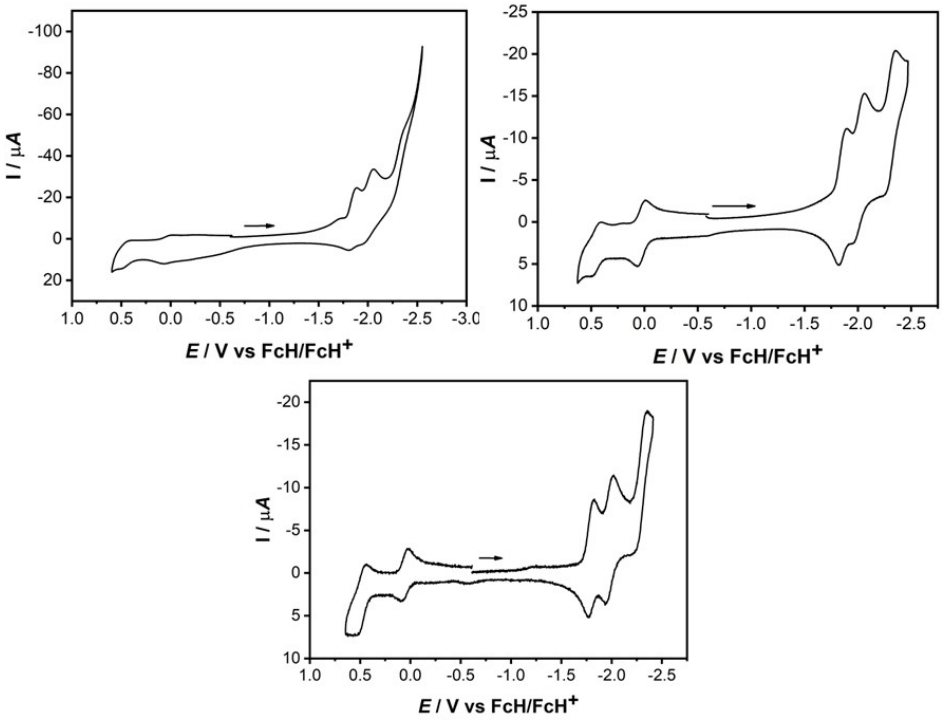

Figure 3. Cyclic voltammograms of **Ru_2** (top left), **Ru_3** (top right), and **Ru_4** (bottom) in acetonitrile with 0.1 M NBu_4PF_6 as a supporting electrolyte. Scan rate: 100 mV/s, glassy carbon working electrode, electrochemical potentials were referenced against Fc/FcH^+ redox couple.

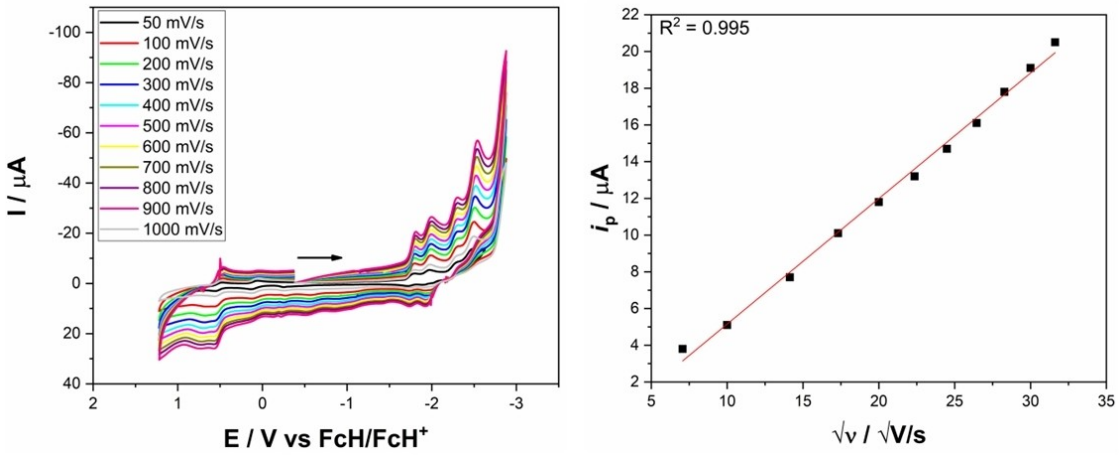

Figure 4. Cyclic voltammograms of **Ru_4** in acetonitrile containing 0.1 M $^nBu_4PF_6$ at different scan rates (left). Diagram on the right depicts variation of peak current (i_p) against the square root of the scan rate for the first reduction waves (Conditions: GC working electrode, platinum wire as a counter electrode, and Fc/FcH^+ couple as an internal reference).

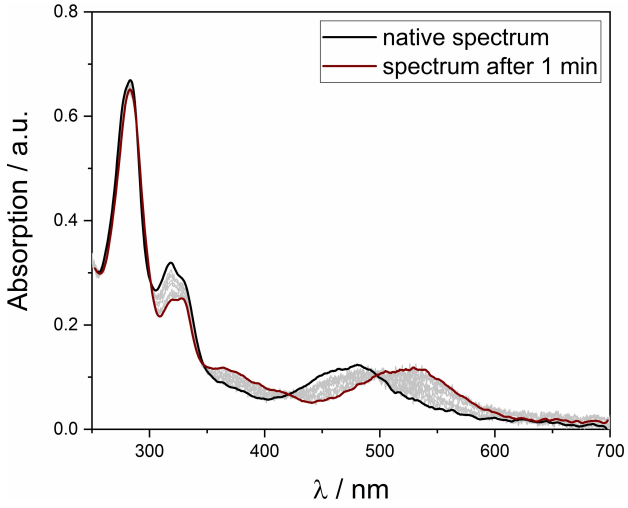

Figure 5. Changing of the UV/Vis spectrum of **Ru_4** after dissolving in MeCN at room temperature.

mixture of a ligand to ligand charge transfer (LLCT) and an inter-ligand charge transfer (ILCT) between the tpy -and MIC unit. Following this observations, the purple solution can be assigned to the Ru complex with a chloride ligand (**Ru_4**), while the orange solution is the Ru complex with an attached acetonitrile (**Ru_5**) which is formed due to a light induced exchange. Further proof for this transformation was obtained from ^{1}H NMR spectroscopy (Figure S17) and mass spectrometry. UV/Vis-SEC measurements of the two oxidation -and the three reduction processes of **Ru_4** were performed in an optically transparent thin layer electrochemical (OTTLE) cell in acetonitrile. In the first oxidation, which is entirely metal based (Ru(II)→Ru(III)), a small red shift and loss of intensity of the band at 545 nm were observed. After reoxidation, the spectra are in complete agreement with the initial spectra, indicating a fully reversible process. During the second oxidation, the MLCT band disappears completely and again, the process is reversible. DFT calculations corroborate the hypothesis that the oxidation is metal based (Figure S41). The first reduction leads to a red shift of the band at 326 nm by 30 nm. After reoxidation, the observed spectrum is comparable to the initial spectrum. From the spin density plots, it is clear that the reduction is manly based on the substituted tpy ligand (Figure S41). In the second reduction, the absorption is broadened in the visible region with a maximum at 410 nm. Comparing the initial and final spectra indicates, that this process is not fully reversible, as indicated by a loss of intensity in the UV region. The spin density plot shows, that the reduction occurs at the terpyridine ligand (Figure S41). The third reduction at −2.29 V is also fully reversible, with only minor changes in the visible region and a blue shift of 20 nm of the band at 283 nm. Analysis of the spin density plot of the reduced species also indicate predominant contribution of the terpyridine centre towards reduction (Figure S41).

Electrocatalytic CO_2 reduction

The catalytic activity of the complexes (**Ru_2**, **Ru_3**, and **Ru_4**) was studied in acetonitrile solution containing 0.1 M NBu_4PF_6 under a CO_2 atmosphere. When the CVs of complexes **Ru_2**, **Ru_3**, and **Ru_4** were measured in CO_2-saturated acetonitrile solution, a significant increase in current beyond the potential −2.1 V versus Fc/Fc^+ was observed, indicating a catalytic process (Figure 6(a)). A closer look at the voltammograms showed that the potential of the first reduction process under a CO_2 atmosphere remained relatively unaffected, with no noticeable change in the peak current as compared to measurements under Ar (Figure 6(a)). However, the cathodic waves become increasingly irreversible after the first reduction along with significant enhancement in catalytic current. This is indicative of a chemical reaction following the electron transfer process.

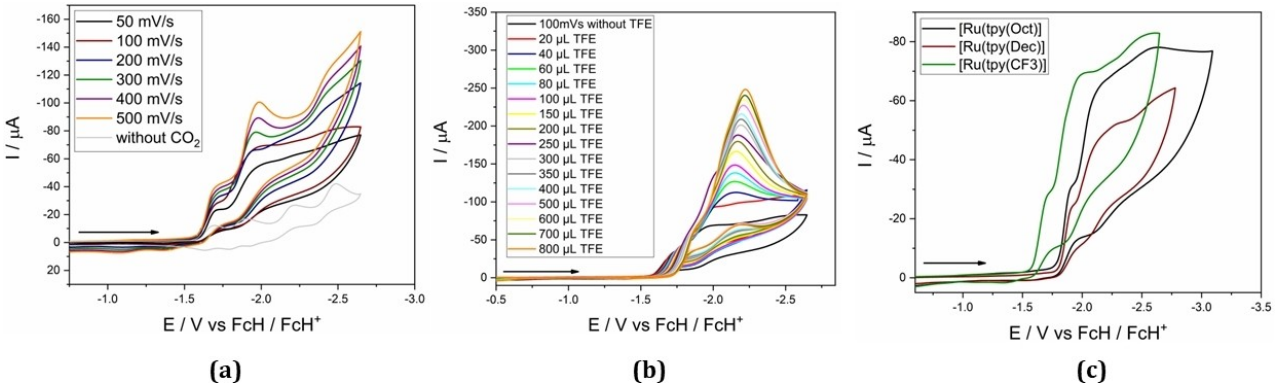

Figure 6. Cyclic voltammograms of **Ru_4**: (a) under Ar (grey trace) and CO_2 atmosphere at different scan rates, (b) upon addition of increasing concentration of TFE in the CO_2 saturated solution. (c) Comparison of onset potentials of the complexes under investigation.

Since the first reduction step is assigned to a reduction at the terpyridine backbone (see electrochemistry and UV/Vis-SEC section) the binding of CO_2 to the Ru(II) centre can be attributed to the chemical reaction, which is largely responsible for the enhancement of the cathodic current following an EC mechanism. Comparison of the onset potentials for the catalytic process in the case of **Ru_2** and **Ru_3** (−1.80 and −1.81 V, respectively) revealed insignificant changes (Figure 6(c)). Conversely, under identical experimental conditions for the corresponding **Ru_4**, the onset potential (−1.59 V) showed an anodic shift of ~200 mV with a half-wave potential of −1.76 V versus Fc/FcH^+. The possible reasons for the decrease in the onset potential in **Ru_4** compared to the long-chain analogues (**Ru_2**, and **Ru_3**) could be due to the better solubility of **Ru_4** compared to **Ru_3**, leading to better interactions with CO_2 in solution, as reported previously.[28] Considering the thermodynamic potential for CO_2 reduction in acetonitrile reported in the literature (−1.28 V versus Fc/FcH^+), an overpotential of 480 mV was calculated for **Ru_4**, which is significantly lower than for the other two complexes (529 and 530 mV for **Ru_2** and **Ru_3**, respectively).[29] Thus, the overpotential for CO_2 reduction can be significantly influenced by changing the substituents on the typ ligand. Due to the lower overpotential observed for catalytic reduction, further discussions will be limited to the catalytic properties of the complex **Ru_4**.

The use of 2,2,2-trifluoroethanol (TFE) as a proton source resulted in further enhancement of the irreversible cathodic current (Figure 6(b)), that followed a linear relationship with increasing concentrations of TFE, indicating a first-order rate dependence (Figure 7(b)). In addition, the linear increase in the value of $(i_{cat}/i_p)^2$ with TFE also indicates first-order reaction kinetics (Figure 7(c)).

However, the deviation of the cathodic wave from the ideal *S*-shaped diagram as predicted by Savéant and co-workers[30] under limiting scan rates ($\nu > 300$ mV/s) and concentrations of TFE precluded extraction of the kinetic parameters. Therefore, the maximum turnover frequency (TOF_{max}) was determined from the slope of i_{cat}/i_p vs. $\nu^{-1/2}$ as 14.07 s^{-1} (Figure S45).[31] On the other hand, the overall catalytic rate constant calculated for the catalytic process was 3.17 s^{-1} (Figure S24, see Supporting Information). Although a direct comparison of molecular catalysts for CO_2 reduction is not recommended, given the role of various competitive factors,[32] the catalyst studied here (**Ru_4**) can be considered a reasonably active catalyst based on the elucidated kinetic parameters.

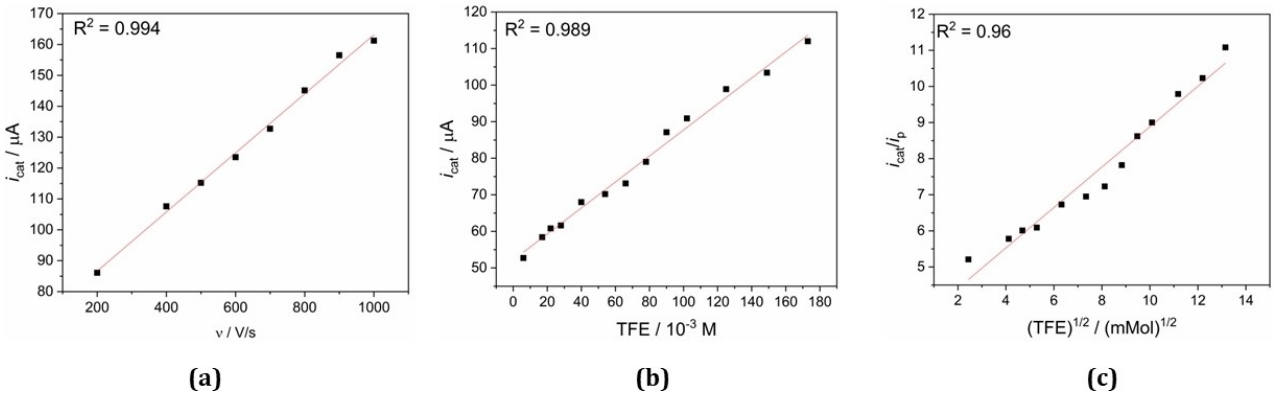

Figure 7. Plot of catalytic currents (i_{cat}) of 0.5 mM **Ru_4** versus (a) scan rates and (b) the concentration of TFE. Diagram (c) depicts the variation of (i_{cat}/i_p) with the square root of the concentration of TFE.

The products formed during the catalytic process were evaluated by controlled potential electrolysis at −1.74 V versus. Fc/FcH+ in anhydrous acetonitrile in the presence of 10% TFE, followed by gas chromatographic analysis of the gaseous reaction mixture (Figure S30). Electrolysis of the 0.05 mM acetonitrile solution of catalyst **Ru_4** for 1.5 h resulted in the consumption of 1.91 C of charge along with selective production of 8.99 μmol of CO with a faradaic efficiency of 92% (see Supporting Information). Further analysis of the reaction mixture revealed an almost negligible amount of H_2 production during the electrolysis process indicating selectivity of the catalyst towards CO (Figure S30). The formation of HCOOH could also be ruled out, as no characteristic peak corresponding to formate appeared in the ^{1}H NMR spectra of the solution after electrolysis (Figure S16).

Various control experiments were performed to rule out adverse effects of any side- phenomena in the catalytic process. UV/Vis spectra of the catalyst solution recorded before and after electrolysis show no change in the position of the absorption maxima, demonstrating the integrity of the core molecular structure of the catalysts (Figure S39). To exclude any effects of catalyst decomposition during electrolysis, rinse test was performed. The absence of any catalytic current beyond the background rules out any role of physically adsorbed species in catalysis (Figure S23). Furthermore, the SEM/EDX analysis of the working electrode after electrolysis showed the absence of ruthenium nanoparticles, ruling out any possible involvement of the nanoparticles in catalysis (Figure S31).[33] Since the presence of a proton source (TFE) can in some cases negatively affect the catalytic process by decomposition of the catalysts, an acid stability test was performed by monitoring the UV/Vis spectra of the 1:1 acetonitrile/TFE solution of the catalyst for 72 h (Figure S35). Identical electronic spectra during the experiment illustrated the stability of the catalysts in the presence of a proton source.

The plausible mechanism of the catalytic reaction was investigated by spectroelectrochemical, FTIR, and NMR studies of the intermediates of the catalyst **Ru_4** under investigation. Since the irreversible cathodic wave occurs after the first reduction process, it can be assumed that one electron reduced species is involved in the catalytic reduction. The spectroelectrochemical analysis described above clearly indicates the participation of terpyridine in the first reduction step. Since the exchange of chloride ion with acetonitrile takes place instantaneously, $[Ru(tpy)(MIC)CH_3CN]^{2+}$ (**Ru_5**) can be assigned as a key species involved in the catalytic process. Electrochemical measurements were also performed with the corresponding $[Ru(tpy)(MIC)CH_3CN]^{2+}$ (**Ru_5**) in CH_3CN with both NBu_4PF_6 and NBu_4Cl as a supporting electrolyte under CO_2 atmosphere. The response of the catalysts **Ru_5** in NBu_4Cl was found to agree well with the observation noted with **Ru_4** in NBu_4PF_6 indicating the significance of a prequilibrium (**Ru_4**↔**Ru_5**) between chloride and acetonitrile solvated complex in the catalytic activity (Figure S28).[34] A precatalytic wave before the irreversible cathodic wave at −1.59 V could probably be assigned to the exchange between chloride and acetonitrile ligand, which results in a shift of the onset potential (Figure S28). Moreover, it was observed that the electrochemical response of **Ru_5** under CO_2 atmosphere was more pronounced in the presence of NBu_4Cl than NBu_4PF_6, suggesting that a higher concentration of chloride ions facilitates the catalytic process (Figure S28(a)). Importantly in the spectroelectrochemical analysis, the UV/Vis/NIR spectra of the acetonitrile solutions of **Ru_4** under Ar and CO_2 environments at open circuit potential (−0.23 V) revealed no difference in the position of absorption bands at 545 nm, which rules out any side reaction or decomposition under CO_2 atmosphere. Now, based on the spectroelectrochemical analysis of **Ru_4** in acetonitrile under Ar (Figure S34, see **UV/Vis-SEC** section), the one electron reduced form of the acetonitrile complex can be formulated as $[Ru(tpy^{\bullet-})(MIC)CH_3CN]^+$. Upon electrolysis of the CO_2 saturated solution **Ru_4** at −1.75 V, a blue shift of the absorption band to 445 nm was observed. Analysis of this solution by IR spectroscopy showed the formation of new bands at 1620 and 1670 cm^{-1}, which could be assigned to the carbonyl stretching frequencies of HCO_3^- (Figure S40).[35] However, the formation of HCOOH, and HCHO, was not detected in either the IR or the NMR spectra of the solution. Notably, electrolysis of the CO_2 saturated solution of **Ru_4** containing 150 μL of TFE did not show peaks corresponding to HCO^{3-} in the IR spectroscopy. However, controlled potential electrolysis of the CO_2 saturated acetonitrile solution of **Ru4** containing 0.1 M NBu_4PF_6 and TFE at −1.75 V over a period of 30 min resulted in the appearance of a band at 2008 cm^{-1}, which is characteristic of Ru-CO stretching vibrations (Figure S38). Based on these observations, we can say that in the absence of TFE, $[Ru(tpy)(MIC)CO_2^{\bullet-}]$ forms Ru-CO via disproportionation reaction with CO_2. While, in the presence of proton source, i.e. TFE, the ruthenium carboxylate intermediate $[Ru(tpy)(MIC)CO_2^{\bullet-}]$, forms the Ru-CO species through the ruthenium-hydroxycarbonyl ($[Ru(tpy)(MIC)COOH]^+$) intermediate (Figure S40). In accordance with all the observations, the plausible mechanistic pathway for the **Ru_4** catalysed CO_2 reduction can be described as follows (Scheme 3).[36] The Ru-CO_2 adduct $[Ru(tpy)(MIC)CO_2^{\bullet-}]^+$ formed from the binding of CO_2 (Steps **c**), undergoes reduction (Steps **d**) followed by a formation of ruthenium-hydroxycarbonyl ($[Ru(tpy)(MIC)COOH]^+$) intermediate in the presence of TFE (Steps **e**). The hydroxycarbonyl intermediate upon subsequent protonation and dehydration (Steps **f**) leads to the formation of metal-carbonyl ($[Ru(tpy)(MIC)CO]^{2+}$) intermediate, which is followed by a reduction and ligand exchange to complete the cycle.

Conclusion

In summary, we have reported here the synthesis and characterization of five Ru(II) complexes (**Ru_2**-**Ru_6**) bound with terpyridines with different PFC tails, a bis-MIC ligand and different monodentate ligands. A detailed study of the optical properties showed, that in acetonitrile the chloride ligand is immediately exchanged by a solvent molecule. A combination of DFT calculations and UV/Vis-SEC measurements showed that both oxidations are reversible and metal-based, whereas the first two reductions occur at the tpy ligand. The catalytic activity for the

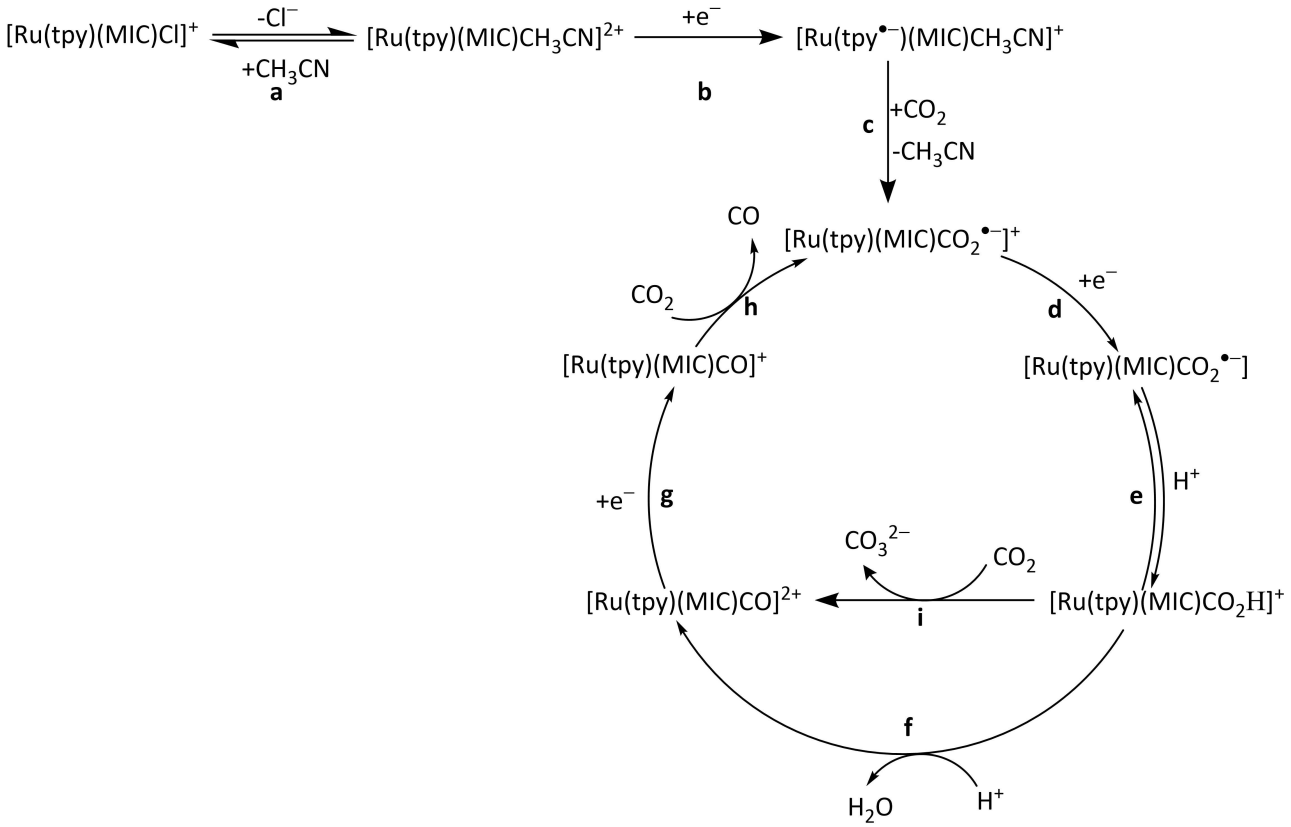

Scheme 3. Possible reaction mechanism for the electrocatalytic CO_2 reduction.

electrochemical CO_2 reduction in the presence of TFE as a proton source was investigated for all complexes. Based on the lower onset potential of **Ru_4** by 200 mV compared to the other two complexes, **Ru_4** was used for a detailed investigation of electrochemical CO_2 reduction. With that complex, a faradaic efficiency of 92% and a turnover frequency (TOF_{max}) of 14.07 s^{-1} were achieved. Based on control experiments, the formation of hydrogen and HCOOH could be excluded. The stability of the catalyst was also demonstrated by UV/Vis experiments and SEM/EDX analysis. A combination of UV/Vis and IR spectroscopy shows that in the presence of a proton an ECE mechanism is followed. We have demonstrated here that tpy centered reductions can be used to open up electrocatalytic CO_2 reduction pathways at the bound metal centre, and the overpotential for CO_2 reduction can be controlled via remote substitution at the tpy ligands. Additionally, we have shown that the strongly donating MIC ligands are helpful in generating favourable kinetic parameters in electrocatalytic CO_2 reduction. Considering the steric and electronic tuning that are synthetically possible for both terpyridine and MIC ligands, we believe that the results presented here will be useful for orthogonal tuning of thermodynamic and kinetic parameters for electrocatalytic CO_2 reduction by combining these two ligand classes within the same catalyst platform.

Experimental Section

General experimental considerations and instrumentation: Unless otherwise noted, all reactions were carried out using standard Schlenk-line techniques under an inert atmosphere of argon (Linde, HiQ Argon 5.0, purity $\geq$ 99.999%) or in a MBraun Unilab SP GloveBox. Commercially available chemicals were used without further purification. THF and diethyl ether were dried and distilled from sodium/benzophenone. Other solvents were available from MBRAUN MB-SPS-800 solvent system. For the synthesis part, all solvents were degassed by standard techniques prior to use. For NMR, $CDCl_3$ was passed through a small plug basic alumina.^{1}H NMR and $^{13}C\{^1H\}$ spectra were recorded on JEOL ECS/ECZ 400/400R spectrometer and JEOL ECZ 400R spectrometer at room temperature. Kinetic NMR spectra were recorded in Fourier transform mode with a Bruker AVANCE 500 spectrometer at 298 K. Chemical shifts are reported in ppm (relative to the TMS signal) with reference to the residual solvent peaks.[37] Multiplets are reported as follows: singlet (s), doublet (d), triplet (t), quartet (q), quintet (quint), and combinations thereof. Mass spectrometry was performed on an Agilent 6210 ESI-TOF. UV/Vis/NIR spectra were recorded with an on a J&M TIDAS spectrometer instrument.

X-ray data were collected on a Bruker D8Venture system at 100(2) K, using graphite-monochromated $Mo_{K\alpha}$ radiation (λ_α = 0.71073 Å). The strategy for the data collection was evaluated by using the APEX3 software. The data were collected by $\omega+\phi$scan techniques and were scaled and reduced using Saint+ and SADABS software. The structures were solved by intrinsic phasing methods using SHELXT-2014/7. The structure was refined by full matrix least-squares usingSHELXL-2014/7, refining on F2. Non-hydrogen atoms were refined anisotropically.[38] The contribution of disordered

solvent molecules to the diffraction pattern was subtracted from the observed data by the "SQUEEZE" method as implemented in PLATON.[39] Deposition Numbers CSD2203803 (for **Ru_4**) and CSD2203804 (for **Ru_5**) contain the supplementary crystallographic data for this paper. These data are provided free of charge by the joint Cambridge Crystallographic Data Centre and Fachinformationszentrum Karlsruhe Access Structures service.

Electrochemistry: Cyclic voltammograms were recorded with a PalmSens4 potentiostat or with a Metrohm Autolab PGSTAT101 by working in anhydrous and degassed acetonitrile (MeCN) with 0.1 M $^{N}Bu_4PF_6$ (dried, >99.0%, electrochemical grade, Fluka) as the supporting electrolyte. A three-electrode setup was used with a glassy carbon working electrode, a coiled platinum wire as counter electrode, and a coiled silver wire as a pseudoreference electrode. The ferrocene/ ferrocenium couple was used as an internal reference.[40]

Bulk electrolysis measurements were performed in a two-compartment cell divided by microporous membrane (Celgard® 2325). A 0.05 mM MeCN solution of **Ru_4** containing 0.1 M $^{N}Bu_4PF_6$ and 0.1 M of TFE was sparged with argon before measurements. The measurements were performed with a Glassy (Vitreous) Carbon rod electrode – GCR 6/60 mmas a working electrode, coiled platinum wire as a counter electrode and a coiled silver wire as a pseudoreference electrode. Samples of the headspace (500 µL) were taken using a gastight syringe (Hamillton). The headspace composition was analyzed using a gas chromatograph equipped with a shincarbon column and a TCD detector using helium as a carrier gas for CO and Ar for the detection of H_2.

Density functional theory: All calculations were performed with the ORCA program package, versions 4.0.1.2 and 4.2.8.[41] The geometries of all species were optimized using the PBE0 functional,[42] the def2-SVP basis sets on all atoms except for Ru, for which the def2-TZVP basis set was used.[43] Solvation was taken into account using the using the SMD method together with the CPCM model[44] using MeCN as solvent, and dispersion corrections were included using the D3 dispersion correction model.[45] The resolution-of-the identity (RI) approximation,[46] with matching basis sets,[47] as well as the RIJCOSX approximation (combination of RI and chain-of-spheres algorithm for exchange integrals) were used to reduce the time of calculations. Numerical frequencies calculations were used in order to check that the optimized structures were local minima and to obtain Gibbs free enthalpies. To obtain more reliable energetics single-point calculations were performed using the optimized geometries, the PBE0 functional and def2-TZVP basis sets on all atoms. Low-lying excitation energies were calculated with time-dependent DFT (TD-DFT). For all calculations spin densities were calculated according to the Löwdin population analysis.[48] Broken-symmetry calculations[48,49] were carried out using optimized geometry to evaluate the exchange coupling constants. Plots of spin-densities and optimized geometries were performed using Chemcraft.[50]

Synthesis

[Ru(tpy-O–$(CH_2)_2$–$(CF_2)_5$–CF_3)(bicarbene)(Cl)] (Ru_2): **Ru_1** (36.6 mg, 0.05 mmol 1 equiv.) and tpy-O–$(CH_2)_2$–$(CF_2)_5CF_3$ **(L_1)** (33.5 mg, 0.05 mmol, 1.0 equiv.) were dissolved in DMSO (1.5 mL) and the solution was purged with argon for 5 min. The mixture was stirred at 120 °C for 16 h. The DMSO was evaporated under high vacuum and **Ru_2** was purified via column chromatography (neutral Alox, DCM:MeOH = 100:1) to give the product as a deep purple solid (41.2 mg, 0.032 mmol, 65%).

^{1}H NMR (400 MHz, CD_3CN): δ = 8.29 (m, 2H, CH_{arom}), 8.17 (m, 2H, CH_{arom}), 8.08 (s, 2H, CH_{arom}), 7.95 (m, 2H, CH_{arom}), 7.91 (m, 4H, CH_{arom}), 7.58 (m, 3H, CH_{arom}), 7.31 (m, 2H, CH_{arom}), 7.24 (m, 3H, CH_{arom}), 7.06 (m, 2H, CH_{arom}), 6.36 (m, 2H, CH_{arom}), 4.73 (s, 3H, N-CH_3), 4.48 (s, 3H, N-CH_3), 4.44 (t, J = 6.26 Hz 2H, CH_2), 2.79 (t, J = 6.76 Hz 2H, CH_2) ppm. ^{13}C NMR (176 MHz, $(CD_3)_2CO$): δ = 160.2, 160.4, 157.0, 144.6, 142.4, 141.5, 140.3, 138.7, 135.8, 130.8, 130.2, 130.0, 129.8, 129.0, 127.6, 127.1, 126.5, 126.1, 124.1, 119.1, 116.2, 115.7, 61.1, 40.3, 40.2, 31.6 ppm. ^{19}F NMR (376 MHz, $(CD_3)_2CO$): δ = -68.59, −70.47, −78.18, −110.19, −118.85, −119.92, −120.58, −123.26 ppm .HRMS(ESI): m/z calc. 1124.1411 (M^+), found 1124.1262 (M^+).

[Ru(tpy-O–$(CH_2)_2$–$(CF_2)_7$–CF_3)(bicarbene)(Cl)] (Ru_3): **Ru_1** (36.6 mg, 0.05 mmol 1 equiv.) and tpy-O–$(CH_2)_2$–$(CF_2)_5CF_3$ **(L_2)** (38.6 mg, 0.05 mmol, 1.0 equiv.) were dissolved in DMSO (1.5 mL) and the solution was purged with argon for 5 min. The mixture was stirred at 120 °C for 16 h. The DMSO was evaporated under high vacuum and **Ru_3** was purified via column chromatography (neutral Alox, DCM:MeOH = 100:1) to give the product as a deep purple solid (33.5 mg, 0.025 mmol, 49%).

^{1}H NMR (400 MHz, CD_2Cl_2): δ = 8.26 (m, 2H, CH_{arom}), 8.16 (m, 2H, CH_{arom}), 8.05 (s, 2H, CH_{arom}), 7.93 (m, 2H, CH_{arom}), 7.90 (m, 4H, CH_{arom}), 7.60 (m, 3H, CH_{arom}), 7.31 (m, 2H, CH_{arom}), 7.22 (m, 3H, CH_{arom}), 7.06 (m, 2H, CH_{arom}), 6.37 (m, 2H, CH_{arom}), 4.69 (s, 3H, N-CH_3), 4.47 (s, 3H, N-CH_3), 4.45 (t, J = 6.99 Hz 2H, CH_2), 2.79 (t, J = 6.81 Hz 2H, CH_2) ppm.^{13}C NMR (176 MHz, $(CD_3)_2CO$): δ = 189.9, 183.1, 160.2, 160.0, 159.3, 157.1, 156.9, 156.3, 148.1, 144.6, 142.4, 141.5, 140.4, 138.7, 135.7, 130.8, 130.1, 130.1, 129.9, 129.8, 129.0, 128.4, 127.6, 127.1, 126.2, 126.1, 124.33 120.1, 119.1, 116.2, 115.6, 61.1, 40.3, 40.2, 31.6 ppm. ^{19}F NMR (376 MHz, $(CD_3)_2CO$): δ = -68.35, −70.23, −78.32, −110.13, −118.75, −119.02, −119.88, −120.59, −123.34 ppm. HRMS(ESI): m/z calc. 1224.1347 (M^+), found 1224.1297 (M^+).

[Ru(tpy-OCF_3)(bicarbene)(Cl)] (Ru_4): **Ru_1** (65.15 mg, 0.11 mmol 1 equiv.) and tpy-O-CF_3 **(L_3)** (36.87 mg, 0.169 mm0 l, 1.6 equiv.) were dissolved in DMSO (2 mL) and the solution was purged with argon for 5 min. The mixture was stirred at 120 °C for 16 h. The DMSO was evaporated under high vacuum and **Ru_4** was purified via column chromatography (neutral Alox, DCM:MeOH = 100:1) to give the product as a deep purple solid (89.3 mg, 0.09 mmol, 82%).

^{1}H NMR (400 MHz, CD_2Cl_2): δ = 8.03 (m, 6H, CH_{arom}), 7.81 (s, 2H, CH_{arom}), 7.71 (m, 4H, CH_{arom}), 7.47 (m, 2H, CH_{arom}), 7.37 (m, 2H, CH_{arom}), 7.20 (m, 3H, CH_{arom}), 6.97 (m, 2H, CH_{arom}), 6.30 (m, 2H, CH_{arom}), 4.81 (s, 3H, N-CH_3), 4.50 (s, 3H, N-CH_3). ppm.^{13}C NMR (176 MHz, $(CD_3)_2CO$): δ = 191.1, 186.1, 159.8, 157.6, 156.1, 150.4, 146.5, 143.6, 142.4, 141.4, 140.2, 138.8, 137.5, 135.9, 130.3, 130.4, 130.1, 129.9, 129.0, 127.6, 127.3, 126.2, 124.0, 123.9, 122.2, 119.6, 40.4, 40.3. ppm. ^{19}F NMR (376 MHz (CD_3CN): δ = -58.45, −72.06, −73.94 ppm. Anal. Calcd. for Ru C_{40} H_{30} N_9 O P F_9 Cl: C, 48.47; H, 3.03; N, 12.72. Found: C, 48.11; H, 3.274; N, 12.55. HRMS(ESI): m/z calc. 846.1257 (M^+), Found 846.1319 (M^+).

[Ru(tpy-OCF_3)(bicarbene)(MeCN)] (Ru_5): **Ru_4** (20.0 mg, 0.02 mmol, 1 equiv.) and $AgPF_6$ (5.6 mg, 0.022 mmol, 1.1 equiv.) were suspended in MeCN (5 mL) and stirred overnight under exclusion of light. The orange solution with white precipitate was filtered over celite. After evaporation of the solvent, the crude mixture was recrystallized in MeCN and Et_2O. **Ru_5** was obtained as an orange solid (22 mg, 0.0195 mmol, 95%).

^{1}H NMR (250 MHz, CD_3CN): δ = 8.25 (m, 2H, CH_{arom}), 8.17 (s, 2H, CH_{arom}), 8.06 (m, 2H, CH_{arom}), 7.98 (m, 2H, CH_{arom}), 7.91 (m, 3H, CH_{arom}), 7.59 (m, 5H, CH_{arom}), 7.33 (m, 2H, CH_{arom}), 7.23 (m, 1H, CH_{arom}), 7.07 (m, 2H, CH_{arom}), 6.36 (m, 2H, CH_{arom}), 4.71 (s, 3H, N-CH_3), 4.46 (s, 3H, N-CH_3) ppm.^{13}C NMR (176 MHz, $(CD_3)_2CO$): δ = 189.7, 182.9, 161.6, 159.6, 153.4, 149.4, 144.9, 143.4, 143.1, 141.0, 140.4, 139.6, 133.9, 133.2, 132.9, 132.8, 132.6, 131.0, 130.1, 128.7, 127.1, 127.0, 125.1, 124.7, 124.7, 123.3, 123.2, 123.3, 120.3, 42.9, 42.7, 31.8, 5.2, 3.5 ppm. ^{19}F NMR (376 MHz, $(CD_3)_2CO$): δ = -55.16, −68.4,

−70.28 ppm. HRMS(ESI): m/z calc. 426.0917 (M^{2+}), found 426.0912 (M^{2+}).

[Ru(tpy-OCF_3)(bicarbene)(CO)] (Ru_6): **Ru_5** (25.0 mg, 0.02 mmol, 1 equiv.) was suspended in Ethanol (10 mL) and CO gas was bubbled through the solution at 0 °C for 10 min. The suspension was stirred overnight under exclusion of light at 70 °C. The yellow solution with yellow precipitate was filtered over celite and washed with cold ethanol. **Ru_6** was obtained as a yellow solid (16 mg, 0.014 mmol, 71 %).

^{1}H NMR (500 MHz, CD_3CN): δ = 8.34 (m, 2H, CH_{arom}), 8.22 (s, 2H, CH_{arom}), 8.10 (m, 2H, CH_{arom}), 8.05 (m, 2H, CH_{arom}), 7.98 (m, 2H, CH_{arom}), 7.87 (m, 2H, CH_{arom}), 7.63 (m, 5H, CH_{arom}), 7.43 (m, 2H, CH_{arom}), 7.23 (m, 1H, CH_{arom}), 7.10 (m, 2H, CH_{arom}) 6.43 (m, 2H, CH_{arom}), 4.73 (s, 3H, N–CH_3), 4.52 (s, 3H, N–CH_3) ppm.^{13}C NMR (176 MHz, $(CD_3)_2CO$): δ = 194.8, 184.2, 178.1, 158.1, 157.4, 155.6, 150.5, 141.7, 140.5, 138.9, 137.0, 135.6, 132.3, 131.3, 131.0, 130.8, 130.6, 129.0, 128.0, 126.08, 124.7, 122.8, 122.2, 41.1, 40.9 ppm. HRMS(ESI): m/z calc. 984.1160 (M^+), found 984.1162 (M^+).

Acknowledgements

Dr. Anja Wiesner is kindly acknowledged for the help by structural solution of the crystal of complex **Ru_4 and Ru_5**. We would like to acknowledge the assistance of the Core Facility BioSupraMol supported by the DFG. Funded by the Deutsche Forschungsgemeinschaft [DFG, German Research Foundation – Project-IDs 358283783 – SFB 1333/2 2022 and 387284271 – SFB 1349]. Arijit Singha Hazari kindly acknowledges funding from the European Union's Horizon 2020 research and innovation programme under the Marie Skłodowska-Curie grant agreement No. 894082. The authors acknowledge support by the state of Baden-Württemberg through bwHPC and the German Research Foundation (DFG) through grant no INST 40/575-1 FUGG (JUSTUS 2 cluster). Open Access funding enabled and organized by Projekt DEAL.

Conflict of Interest

The authors declare no conflict of interest.

Data Availability Statement

The data that support the findings of this study are available in the supplementary material of this article.

Keywords: CO_2 reduction · mesoionic carbenes · ruthenium · spectroelectrochemistry · terpyridine

[1] a) K. J. Lee, N. Elgrishi, B. Kandemir, J. L. Dempsey, *Nat. Chem. Rev.* **2017**, *1*, 6879–6893; b) J. L. Dempsey, A. J. Esswein, D. R. Manke, J. Rosenthal, J. D. Soper, D. G. Nocera, *Inorg. Chem.* **2005**, *44*, 6879–6892.
[2] E. E. Benson, C. P. Kubiak, A. J. Sathrum, J. M. Smieja, *Chem. Soc. Rev.* **2009**, *38*, 89–99.
[3] a) M. D. Kärkäs, O. Verho, E. V. Johnston, B. Åkermark, *Chem. Rev.* **2014**, *114*, 11863–12001; b) N. S. Lewis, D. G. Nocera, *P. Natl. A. Sci. USA* **2006**, *103*, 15729–15735; c) J. R. McKone, S. C. Marinescu, B. S. Brunschwig, J. R. Winkler, H. B. Gray, *Chem. Sci.* **2014**, *5*, 865–878.
[4] J.-M. Savéant, *Chem. Rev.* **2008**, *108*, 2348–2378.
[5] J. Qiao, Y. Liu, F. Hong, J. Zhang, *Chem. Soc. Rev.* **2014**, *43*, 631–675.
[6] a) M. L. Clark, P. L. Cheung, M. Lessio, E. A. Carter, C. P. Kubiak, *ACS Catal.* **2018**, *8*, 2021–2029; b) M. L. Pegis, C. F. Wise, B. Koronkiewicz, J. M. Mayer, *J. Am. Chem. Soc.* **2017**, *139*, 11000–11003; c) I. Azcarate, C. Costentin, M. Robert, J.-M. Savéant, *J. Phys. Chem. C* **2016**, *120*, 28951–28960.
[7] R. Francke, B. Schille, M. Roemelt, *Chem. Rev.* **2018**, *118*, 4631–4701.
[8] S. Gonell, E. A. Assaf, K. D. Duffee, C. K. Schauer, A. J. M. Miller, *J. Am. Chem. Soc.* **2020**, *142*, 8980–8999.
[9] S. Gonell, M. D. Massey, I. P. Moseley, C. K. Schauer, J. T. Muckerman, A. J. M. Miller, *J. Am. Chem. Soc.* **2019**, *141*, 6658–6671.
[10] a) S. Gonell, E. A. Assaf, J. Lloret-Fillol, A. J. Miller, *ACS Catal.* **2021**, *11*, 15212–15222; b) E. A. Assaf, S. Gonell, C.-H. Chen, A. J. Miller, *ACS Catal.* **2022**, *12*, 12596–12606.
[11] a) E. Baranoff, J.-P. Collin, L. Flamigni, J.-P. Sauvage, *Chem. Soc. Rev.* **2004**, *33*, 147–155; b) H. Hofmeier, U. S. Schubert, *Chem. Soc. Rev.* **2004**, *33*, 373–399; c) H.-J. Nie, C.-J. Yao, M.-J. Sun, Y.-W. Zhong, J. Yao, *Organometallics* **2014**, *33*, 6223–6231; d) J. P. Sauvage, J. P. Collin, J. C. Chambron, S. Guillerez, C. Coudret, V. Balzani, F. Barigelletti, L. de Cola, L. Flamigni, *Chem. Rev.* **1994**, *94*, 993–1019; e) U. Schubert, G. R. Newkome, H. Hofmeier, *Modern terpyridine chemistry* Wiley-VCH, Weinheim, **2006**; f) M.-J. Sun, J.-Y. Shao, C.-J. Yao, Y.-W. Zhong, J. Yao, *Inorg. Chem.* **2015**, *54*, 8136–8147.
[12] J. Klein, A. Stuckmann, S. Sobottka, L. Suntrup, M. van der Meer, P. Hommes, H.-U. Reissig, B. Sarkar, *Chem. Eur. J.* **2017**, *23*, 12314–12325.
[13] a) N. Elgrishi, M. B. Chambers, V. Artero, M. Fontecave, *Phys. Chem. Chem. Phys.* **2014**, *16*, 13635–13644; b) N. Elgrishi, M. B. Chambers, M. Fontecave, *Chem. Sci.* **2015**, *6*, 2522–2531; c) N. Elgrishi, S. Griveau, M. B. Chambers, F. Bedioui, M. Fontecave, *Chem. Commun.* **2015**, *51*, 2995–2998.
[14] R. Tatikonda, M. Cametti, E. Kalenius, A. Famulari, K. Rissanen, M. Haukka, *Eur. J. Inorg. Chem.* **2019**, *2019*, 4463–4470.
[15] a) P. Hommes, C. Fischer, C. Lindner, H. Zipse, H.-U. Reissig, *Angew. Chem. Int. Ed.* **2014**, *53*, 7647–7651; *Angew. Chem.* **2014**, *126*, 7778–7782; b) S. Aroua, T. K. Todorova, P. Hommes, L.-M. Chamoreau, H.-U. Reissig, V. Mougel, M. Fontecave, *Inorg. Chem.* **2017**, *56*, 5930–5940.
[16] R. H. Crabtree, *Coord. Chem. Rev.* **2013**, *257*, 755–766.
[17] O. Schuster, L. Yang, H. G. Raubenheimer, M. Albrecht, *Chem. Rev.* **2009**, *109*, 3445–3478.
[18] a) R. Huisgen, G. Szeimies, L. Möbius, *Chem. Ber.* **1967**, *100*, 2494–2507; b) C. W. Tornøe, C. Christensen, M. Meldal, *J. Org. Chem.* **2002**, *67*, 3057–3064; c) V. V. Rostovtsev, L. G. Green, V. V. Fokin, K. B. Sharpless, *Angew. Chem. Int. Ed.* **2002**, *41*, 2596–2599; *Angew. Chem.* **2002**, *114*, 2708–2711; d) H. C. Kolb, M. G. Finn, K. B. Sharpless, *Angew. Chem. Int. Ed.* **2001**, *40*, 2004–2021; *Angew. Chem.* **2001**, *113*, 2056–2075.
[19] a) D. Schweinfurth, N. Deibel, F. Weisser, B. Sarkar, *Nachr. Chem.* **2011**, *59*, 937–941; b) D. Schweinfurth, L. Hettmanczyk, L. Suntrup, B. Sarkar, *Z. Anorg. Allg. Chem.* **2017**, *643*, 554–584.
[20] B. Schulze, U. S. Schubert, *Chem. Soc. Rev.* **2014**, *43*, 2522–2571.
[21] K. F. Donnelly, A. Petronilho, M. Albrecht, *Chem. Commun.* **2013**, *49*, 1145–1159.
[22] a) S. Hohloch, C. Y. Su, B. Sarkar, *Eur. J. Inorg. Chem.* **2011**, *2011*, 3067–3075; b) M. Gazvoda, M. Virant, A. Pevec, D. Urankar, A. Bolje, M. Kočevar, J. Košmrlj, *Chem. Commun.* **2016**, *52*, 1571–1574; c) R. Maity, S. Hohloch, C.-Y. Su, M. van der Meer, B. Sarkar, *Chem. Eur. J.* **2014**, *20*, 9952–9961; d) A. Petronilho, M. Rahman, J. A. Woods, H. Al-Sayyed, H. Müller-Bunz, J. M. Don MacElroy, S. Bernhard, M. Albrecht, *Dalton Trans.* **2012**, *41*, 13074–13080.
[23] a) S. Friães, S. Realista, C. S. B. Gomes, P. N. Martinho, B. Royo, *Molecules* **2021**, 26–39; b) L. Suntrup, F. Stein, J. Klein, A. Wilting, F. G. L. Parlane, C. M. Brown, J. Fiedler, C. P. Berlinguette, I. Siewert, B. Sarkar, *Inorg. Chem.* **2020**, *59*, 4215–4227; c) T. Scherpf, C. R. Carr, L. J. Donnelly, Z. S. Dubrawski, B. S. Gelfand, W. E. Piers, *Inorg. Chem.* **2022**, *61*, 13644–13656; d) M. van der Meer, E. Glais, I. Siewert, B. Sarkar, *Angew. Chem. Int. Ed.* **2015**, *54*, 13792–13795; *Angew. Chem.* **2015**, *127*, 13997–14000.
[24] G. Meng, L. Kakalis, S. P. Nolan, M. Szostak, *Tetrahedron Lett.* **2019**, *60*, 378–381.
[25] L. Suntrup, S. Hohloch, B. Sarkar, *Chem. Eur. J.* **2016**, *22*, 18009–18018.
[26] Z. Chen, C. Chen, D. R. Weinberg, P. Kang, J. J. Concepcion, D. P. Harrison, M. S. Brookhart, T. J. Meyer, *Chem. Commun.* **2011**, *47*, 12607–12609.

[27] S. Gonell, M. D. Massey, I. P. Moseley, C. K. Schauer, J. T. Muckerman, A. J. M. Miller, *J. Am. Chem. Soc.* **2019**, *141*, 6658–6671.
[28] F. Cheng, J. Zhu, A. Adronov, *Chem. Mater.* **2011**, *23*, 3188–3194.
[29] C. Costentin, S. Drouet, M. Robert, J.-M. Savéant, *Science* **2012**, *338*, 90–94.
[30] J.-M. Saveant, *ChemElectroChem* **2016**, *3*, 1967–1977.
[31] M. E. Ahmed, A. Rana, R. Saha, S. Dey, A. Dey, *Inorg. Chem.* **2020**, *59*, 5292–5302.
[32] E. S. Rountree, B. D. McCarthy, T. T. Eisenhart, J. L. Dempsey, *Inorg. Chem.* **2014**, *53*, 9983–10002.
[33] K. J. Lee, B. D. McCarthy, J. L. Dempsey, *Chem. Soc. Rev.* **2019**, *48*, 2927–2945.
[34] H. Shirley, M. T. Figgins, C. M. Boudreaux, N. P. Liyanage, R. W. Lamb, C. E. Webster, E. T. Papish, J. H. Delcamp, *ChemCatChem* **2020**, *12*, 4879–4885.
[35] E. Oberem, A. F. Roesel, A. Rosas-Hernández, T. Kull, S. Fischer, A. Spannenberg, H. Junge, M. Beller, R. Ludwig, M. Roemelt, R. Francke, *Organometallics* **2019**, *38*, 1236–1247.
[36] a) B. A. Johnson, S. Maji, H. Agarwala, T. A. White, E. Mijangos, S. Ott, *Angew. Chem. Int. Ed.* **2016**, *55*, 1825–1829; b) B. Giri, A. Mahata, T. Kella, D. Shee, F. de Angelis, S. Maji, *J. Catal.* **2022**, *405*, 15–23.
[37] G. R. Fulmer, A. J. M. Miller, N. H. Sherden, H. E. Gottlieb, A. Nudelman, B. M. Stoltz, J. E. Bercaw, K. I. Goldberg, *Organometallics* **2010**, *29*, 2176–2179.
[38] a) *APEX3*, Bruker AXS Inc., Madison, Wisconsin, USA, **2015**; b) G. M. Sheldrick, *SADABS Ver. **2008**/1, Program for Empirical Absorption Correction*, University of Göttingen, Germany, **2008**; c) *SAINT+, Data Integration Engine, Version 8.27b* ©, Bruker AXS Inc., Madison, Wisconsin, USA, 1997–2012; d) G. M. Sheldrick, *SHELXL Version **2014**/7, Program for Chrystal Structure Solution and Refinement*, University of Göttingen, Germany, **2014**; e) C. B. Hübschle, G. M. Sheldrick, B. Dittrich, *J. Appl. Crystallogr.* **2011**, *44*, 1281–1284; f) G. M. Sheldrick, *Acta Crystallogr.* **2008**, *A64*, 112–122; g) G. M. Sheldrick, *Acta Crystallogr.* **2015**, *C71*, 3.17; h) A. L. Spek, *Acta Crystallogr.* **2015**, *C71*, 9–18; i) A. L. Spek, *Acta Crystallogr.* **2009**, *D65*, 148–155; j) A. L. Spek, *J. Appl. Crystallogr.* **2003**, *36*, 7–13.
[39] A. L. Spek, *PLATON*, A multipurpose Crystallographic Tool, Utrecht, the Netherlands, **1998**.
[40] L. Fabbrizzi, *ChemTexts* **2020**, *6*, 1039–1059.
[41] F. Neese, *WIREs Comput. Mol. Sci.* **2018**, *8*, 33–9.
[42] C. Adamo, V. Barone, *J. Chem. Phys.* **1999**, *110*, 6158–6170.
[43] F. Weigend, R. Ahlrichs, *Phys. Chem. Chem. Phys.* **2005**, *7*, 3297–3305.
[44] V. Barone, M. Cossi, *J. Phys. Chem. A* **1998**, *102*, 1995–2001.
[45] a) S. Grimme, *J. Comput. Chem.* **2006**, *27*, 1787–1799; b) S. Grimme, *J. Comput. Chem.* **2004**, *25*, 1463–1473; c) S. Grimme, J. Antony, S. Ehrlich, H. Krieg, *J. Chem. Phys.* **2010**, *132*, 154104–154122; d) S. Grimme, S. Ehrlich, L. Goerigk, *J. Comput. Chem.* **2011**, *32*, 1456–1465.
[46] a) P. Seth, P. L. Ríos, R. J. Needs, *J. Chem. Phys.* **2011**, *134*, 84105–84114; b) F. Neese, G. Olbrich, *Chem. Phys. Lett.* **2002**, *362*, 170–178; c) R. Izsák, F. Neese, *J. Chem. Phys.* **2011**, *135*, 144105–144117; d) J. L. Whitten, *J. Chem. Phys.* **1973**, *58*, 4496–4502; e) O. Vahtras, J. Almlöf, M. W. Feyereisen, *Chem. Phys. Lett.* **1993**, *213*, 514–518; f) F. Neese, F. Wennmohs, A. Hansen, *J. Chem. Phys.* **2009**, *130*, 114108–114126; g) F. Neese, *J. Comput. Chem.* **2003**, *24*, 1740–1747.
[47] a) K. Eichkorn, O. Treutler, H. Öhm, M. Häser, R. Ahlrichs, *Chem. Phys. Lett.* **1995**, *240*, 283–290; b) K. Eichkorn, F. Weigend, O. Treutler, R. Ahlrichs, *Theor. Chem. Acc.* **1997**, *97*, 119–124; c) F. Weigend, *Phys. Chem. Chem. Phys.* **2006**, *8*, 1057–1065.
[48] P.-O. Löwdin, *J. Chem. Phys.* **1950**, *18*, 365–377.
[49] a) D. Doehnert, J. Koutecky, *J. Am. Chem. Soc.* **1980**, *102*, 1789–1796; b) J. Gräfenstein, E. Kraka, M. Filatov, D. Cremer, *Int. J. Mol. Sci.* **2002**, *3*, 360–394; c) F. Neese, *J. Phys. Chem. Solids* **2004**, *65*, 781–785; d) K. Yamaguchi, *Chem. Phys. Lett.* **1975**, *33*, 330–335.
[50] G. A. Zhurko, D. A. Zhurko, ChemCraft, Tool for Treatment of the Chemical Data, http://www.chemcraftprog.com.

Manuscript received: February 7, 2023
Accepted manuscript online: March 27, 2023
Version of record online: April 24, 2023